Journal of Materials Chemistry B

ROYAL SOCIETY OF CHEMISTRY

REVIEW

View Article Online
View Journal | View Issue

Cite this: J. Mater. Chem. B, 2020, 8, 7121

Finely tuned Prussian blue-based nanoparticles and their application in disease treatment

Yong Gao,[a] Guocan Yu,[b] Kuoran Xing,[a] Dmitry Gorin,[c] Yuri Kotelevtsev,[d] Weijun Tong *[a] and Zhengwei Mao *[a]

Received 15th May 2020,
Accepted 23rd June 2020

DOI: 10.1039/d0tb01248c

rsc.li/materials-b

The Prussian blue (PB) based nanostructure is a mixed-valence coordination network with excellent biosafety, remarkable photothermal effect and multiple enzyme-mimicking behaviours. Compared with other nanomaterials, PB-based nanoparticles (NPs) exhibit several unparalleled advantages in biomedical applications. This review begins with the chemical composition and physicochemical properties of PB-based NPs. The tuning strategies of PB-based NPs and their biomedical properties are systemically demonstrated. Afterwards, the biomedical applications of PB-based NPs are comprehensively recounted, mainly focusing on treatment of tumors, bacterial infection and inflammatory diseases. Finally, the challenges and future prospects of PB-based NPs and their application in disease treatment are discussed.

1 Introduction

Prussian blue nanoparticles (PB NPs) are widely studied in catalysis,[1] ion batteries,[2] spectroscopy,[3] chemical sensing[4] and biomedicine.[5] PB was discovered to be a pigment by Diesbach in 1704. The crystal structure of PB was investigated with powder diffraction in 1936 and further determined with single crystal diffraction in 1977.[6,7] Owing to its remarkable adsorption capability for heavy metal ions, PB was approved as an antidote for thallium poisoning by the U. S. Food and Drug Administration in 2003.[8]

PB nanoparticles have a crystalline framework structure mainly composed of Fe^{3+}, Fe^{2+} and bridging cyano groups. In the face-centered cubic unit cell, alternatively arranged Fe^{3+} and Fe^{2+} ions coordinate with bridging cyano groups, generating a 3D coordination network. PB is insoluble due to the 3D coordination network, which makes PB nanoparticles the most common form of PB in biomedicine. The representative Fe(II)–CN–Fe(III) linkage

[a] MOE Key Laboratory of Macromolecular Synthesis and Functionalization, Department of Polymer Science and Engineering, Zhejiang University, Zheda Road 38, Hangzhou 310027, China. E-mail: tongwj@zju.edu.cn, zwmao@zju.edu.cn
[b] Laboratory of Molecular Imaging and Nanomedicine, National Institute of Biomedical Imaging and Bioengineering, National Institutes of Health, Bethesda, MD 20892, USA
[c] Center for Photonics and Quantum Materials, Skolkovo Institute of Science and Technology, Russian Federation
[d] Functional Genomics and RNAi Therapy CREI, Skolkovo Institute for Science and Technology, 3 Nobel Street, Skolkovo Moscow region, 143026, Russian Federation

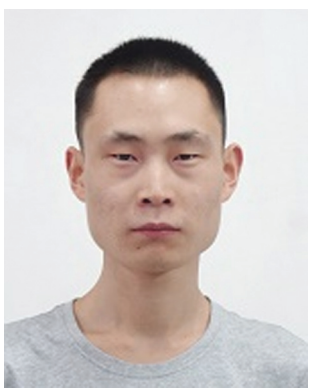

Yong Gao

Yong Gao obtained his BSc degree in Materials Chemistry from Zhengzhou University in 2016. Afterwards, he obtained his MEng degree in Applied Chemistry from South China Normal University in 2019. Now, he is a PhD candidate in Zhejiang University under the supervision of Prof. Zhengwei Mao and Assoc. Prof. Weijun Tong. His research interests are focused on biocompatible coordination polymers and their application in treatment of disease.

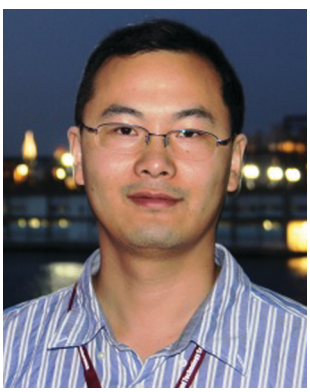

Weijun Tong

Weijun Tong is currently an associate professor of materials science at Zhejiang University. He obtained his PhD in materials science in 2007 under the supervision of Prof. Changyou Gao at Zhejiang University, China, and Prof. Helmuth Möhwald at Max-Planck-Institute of Colloids and Interfaces, Germany. His main scientific interests are in the areas of nanozymes, MOF nanoparticles, and functional colloids and their biomedical applications.

endows PB NPs with an absorbance peak of 700 nm, and thus PB NPs can effectively convert red light and near infrared (NIR) light into heat. The other oxidative states of PB were named as Prussian white, Prussian yellow and Berlin green accordingly. Moreover, the different oxidative states can mutually transform in catalytic reactions, which is the basis of the enzyme-mimicking activities of PB NPs.

PB NPs have demonstrated their potential in the biomedical field. Firstly, the remarkable photothermal effect of PB NPs enables clearance of tumor cells and bacteria under NIR light.[9] Secondly, PB NPs with mesopores or hollow structures can be used to deliver drugs and enzymes to achieve chemotherapy and other therapies. Thirdly, the enzyme-mimicking activities of PB NPs can be used to scavenge reactive oxygen species (ROS) in inflammatory diseases and promote oxygen supply in photodynamic therapy (PDT).[10] Finally, the bioimaging properties of PB-based NPs can be used to monitor the therapeutic efficiency and guide subsequent treatment (Fig. 1).

In this review, we sum up the synthesis and structural tuning of PB NPs in the past decade and focus on the structure–function relationship of these finely tuned PB-based NPs. Secondly, we recount their biomedical application in inflammatory diseases, bacterial infection, diversified tumor therapy and biomedical imaging. Finally, we discuss some innovative design strategies and future research direction of PB-based NPs.

Zhengwei Mao

Zhengwei Mao is currently a professor in the Department of Polymer Science and Engineering at Zhejiang University. He obtained his PhD in materials science in 2007 under the supervision of Prof. Changyou Gao and Prof. Jiacong Shen at Zhejiang University, China. He worked as a postdoc under the guidance of Prof. Dayang Wang and Prof. Helmuth Möhwald at Max Planck Institute of Colloids and Interfaces, Germany. His research is focused on responsive polymeric nanomaterials for controlled drug delivery against inflammation and cancer.

2 Synthesis and structural tuning of PB NPs

2.1 Synthesis of PB NPs

The molecular formula of soluble-type PB is KFe(III)Fe(II)$(CN)_6$. In the lattice of PB, the Fe^{3+} ion and neighboring cyano groups form a $Fe(CN)_6$ cluster. Therefore, the coprecipitation of Fe^{2+} and $Fe(CN)_6^{3-}$ ions in aqueous solution became a typical method to prepare PB NPs.[11] Similarly, PB NPs could also be prepared by coprecipitation of Fe^{3+} and $[Fe(CN)_6]^{4-}$ ions.[12]

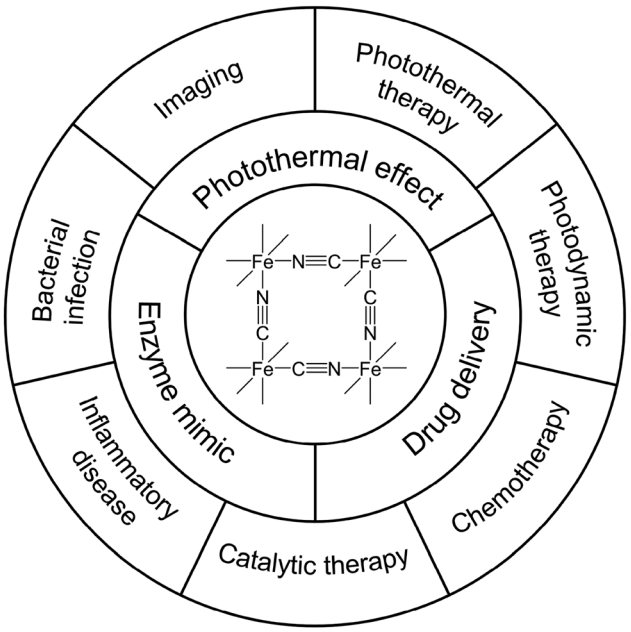

Fig. 1 Schematic illustration of the functionality of PB-based NPs and their biomedical applications.

The second method to prepare PB NPs is by heating $K_3Fe(CN)_6$ and polyvinylpyrrolidone (PVP) in acid solution. $K_3Fe(CN)_6$ releases Fe^{3+} in acid solution, sequentially Fe^{3+} ions are reduced by PVP and they bond with the remaining $K_3Fe(CN)_6$ to generate PB NPs.[13] Generally, PVP acts as a reductant and surfactant. Other surfactants including polysaccharides[14] and polyethylene glycol (PEG)[15] have been applied to replace PVP to prepare PB NPs.

The physicochemical properties of PB NPs are key factors for their biomedical applications. Hence, some novel synthetic technologies were investigated to prepare PB NPs with favorable physicochemical properties. The crystallinity of PB NPs is associated with their magnetic behavior. Considering this, Qin *et al.* applied a magnetic internal heating method to fabricate PB NPs with excellent crystallinity and dispersibility.[16] The alternating-current magnetic field generated a uniform thermal field for PB NP growth, thereby improving the crystallinity and dispersity of PB NPs. Moreover, the resulting PB NPs exhibited elevated magnetic longitudinal relativity due to their higher crystalline integrity. The enzyme-like activity is another physicochemical property tightly associated with nanocatalytic medicine. Komkova *et al.* prepared PB NPs with higher activity than natural peroxidase (POD) *via* catalytic hydrogen peroxide activation.[17] Firstly a $Fe^{III}[Fe^{III}(CN)_6]$ intermediate complex was obtained by coprecipitation of Fe^{3+} and $Fe(CN)_6^{3-}$ ions, then reductive hydrogen peroxide was added to reduce the high-valence intermediate. In this catalytic synthetic approach, PB NPs with outstanding POD-like activity were prepared.

2.2 NPs based on PB analogs and ion doping

The brief cubic structure of PB NPs allows for introducing similar functional metal atoms into the PB lattice. There are

two main approaches to tune the chemical composition of PB NPs, complete substitution (PB analogs) and partial substitution (doping), both of which allow for incorporating new functions and enhancing the existing properties of PB NPs.

PB analogs refer to compounds that are similar in structure to PB in which the C-bonded or N-bonded Fe atoms are completely replaced by similar atoms. The common method to prepare NPs of PB analogs is to alter the precursor. For example, NPs of gallium PB analog $KGa[Fe(CN)_6]\cdot nH_2O$ were synthetized by mixing $Ga(NO_3)_3$ solution with $K_4[Fe(CN)_6]$ solution.[18] NPs of the cobalt PB analog were synthetized by mixing $FeCl_2\cdot 4H_2O$ with $K_3Co(CN)_6$ in aqueous solution.[19] The PB analogs provide structural diversity which expands the biomedical applications of PB-based NPs. For instance, NPs of the manganese PB analog exhibit great potential as a contrast agent in magnetic resonance imaging (MRI) after incorporating manganese. Meanwhile, the Mn–CN–Fe linkage in manganese PB analog is relatively weak and the Mn^{2+} will release in response to an acid environment. The pH-responsive Mn^{2+} release of the manganese PB analog was applied to monitor synchronous drug release in tumor chemotherapy.[20]

Doping refers to partial substitution of Fe atoms with similar atoms; it is another method to prepare PB NPs with tunable properties. Due to the remarkable MRI performance of gadolinium, PB NPs doped with gadolinium exhibit good performance in MRI.[21] Cai *et al.* synthetized hollow mesoporous gadolinium PB NPs with tunable localized surface plasmon resonance (LSPR) (Fig. 2). As the Gd^{3+} amount increased, the absorption peak shifted to 910 nm and the MRI/photoacoustic imaging (PAI) performance was also significantly enhanced.[22]

2.3 Tunable morphology of PB NPs

The morphology is an important consideration of PB NPs in biomedicine. NPs with hollow structures are featured with high drug loading capacity and high reactive activity and allow for developing multifunctional systems. Generally, there are three approaches to prepare hollow PB NPs, *i.e.* mini-emulsion periphery polymerization (MEPP), chemical etching, and template synthesis.

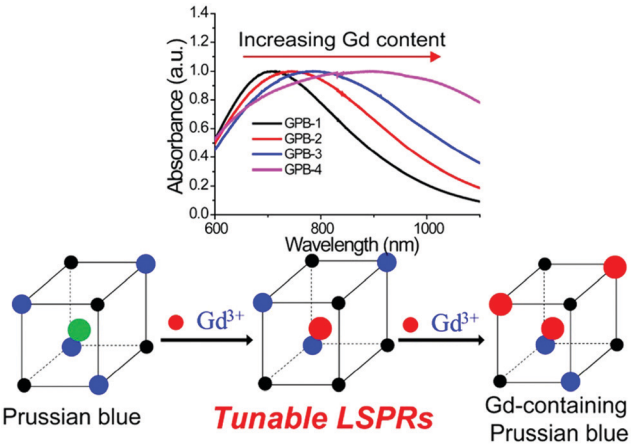

Fig. 2 PB NPs doped with gadolinium and their enhanced properties (adapted with permission from ref. 22. Copyright 2016, American Chemical Society).

In a typical MEPP process, a polymer surfactant capped with pentacyanoferrate groups was employed to form PB nanoshells in a water/toluene mini-emulsion (Fig. 3A).[23] The pentacyanoferrate groups were distributed on the mini-emulsion interface. The added Fe^{3+} initiated the coordination polymerization and PB nanoshells were generated on the mini-emulsion interface. Similarly, emulsion-induced assembly of the amphiphilic pentacyanoferrate block ionomer was used to prepare PB nanocontainers (Fig. 3B).[24]

Chemical etching is another approach to synthesize hollow PB NPs (Fig. 3C).[25] The outer layer of PB mesocrystals was protected by PVP, while the interior of PB mesocrystals was etched by concentrated hydrochloric acid. This is a well-established method to fabricate hollow mesoporous PB (HMPB) NPs with high crystallinity. Furthermore, shell-in-shell PB NPs (Fig. 3D) and PB analog nanoframes (Fig. 3E) were also prepared *via* controlled chemical etching.[26,27]

Template synthesis is also a method to prepare hollow PB NPs. Cai *et al.* used bovine serum albumin (BSA) as the template for Prussian white (a reduced state of PB) preparation.[28] Mn^{2+} and $Fe(CN)_6^{4-}$ combined with the BSA template, and formed hollow manganese Prussian white capsules (HMPWCs, Fig. 3F). Zhang *et al.* synthesized hollow PB nanozymes (HPBZs) with the assistance of bismuth ions.[29] Firstly, bismuth ions bonded with $Fe(CN)_6^{3-}$ and formed a metastable hollow $BiFe(CN)_6$ intermediate. Afterwards, the hollow intermediate acted as a template for PB growth.

Generally, the above-mentioned approaches for preparing hollow PB NPs have their own pros and cons. And the as-prepared PB NPs vary in microstructure. For the MEPP approach, the high cost of the functional precursors limits the scalable preparation, but the meticulous shell-like microstructures have promising academic implication. The acid etching method has been a classical method to prepare HMPB NPs. The HMPB NPs have high crystalline integrity and remarkable photothermal efficiency, which encourages the following microstructural design, including pH-responsive shells constructed on HMPB NPs. The template synthesis is a facile method to prepare hollow PB NPs, but their spherical structure has some notches.

In addition to the hollow structure of PB NPs, other physicochemical properties including particle size and surface roughness are also important factors in the biomedical application of PB NPs. The sizes of most PB NPs are larger than 50 nm, which influences the cell phagocytosis, *in vivo* circulation, and biodistribution of PB NPs. Shou *et al.* prepared ultrasmall PB NPs by zinc doping to alter the growth rate of PB NPs.[30] The diameter of PB NPs was reduced from 38.5 nm to 3.8 nm after doping with 10% zinc (initial molar concentration of zinc ions). Hu *et al.* adjusted the particle size and morphology of PB NPs by altering PVP concentration.[31] The results indicated that smaller PB NPs with rougher surfaces were obtained under lower PVP concentration, while bigger and smoother cubic

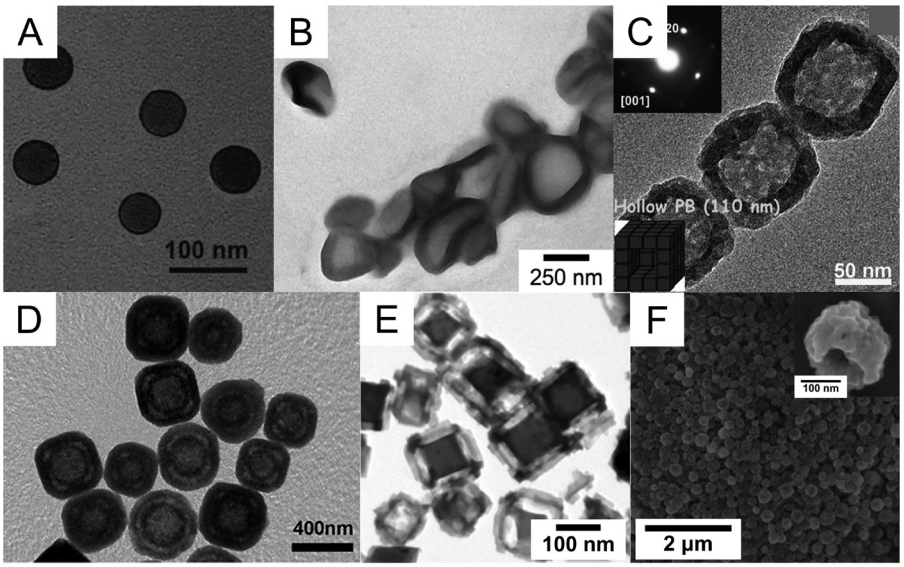

Fig. 3 PB-based NPs with hollow cavities. (A) PB nanoshells (reprinted with permission from ref. 23. Copyright 2009, American Chemical Society). (B) PB nanocontainers (reprinted with permission from ref. 24. Copyright 2011, American Chemical Society). (C) HMPB NPs (reprinted with permission from ref. 25. Copyright 2012, Wiley-VCH). (D) Shell-in-shell PB NPs (reprinted with permission from ref. 26. Copyright 2013, American Chemical Society). (E) PB analog nanoframes (reprinted with permission from ref. 27. Copyright 2016, Wiley-VCH). (F) Hollow manganese Prussian white capsules (reprinted with permission from ref. 28. Copyright 2019, Elsevier).

PB NPs were obtained under higher PVP concentration. Nevertheless, the relationship between the surface roughness and therapeutic efficiency of PB NPs has not been investigated.

2.4 Surface modification of PB NPs

PB NPs exhibit good biosafety and low cytotoxicity in physiological conditions. The physiological stability, biocompatibility and adequate circulation in blood are also required in biomedical applications. As an exogenous component, the PB NPs will be quickly cleared by the immune system, and the reduced circulation time will limit the therapeutic efficiency of PB NPs. Modification with a suitable polymer or cell membrane will effectively extend the circulation time and elevate the immune evasion ability of PB NPs.

Biocompatible polymers including PVP and PEG were applied as surface coatings for PB NPs to promote their physiological stability. For instance, PEG-modified PB cubes and magnetic PB NPs exhibited good physiological stability.[32,33] Hyaluronic acid (HA) is a natural polymer which can bind specifically to the overexpressed CD44 receptor of tumor cells. Therefore, HA coating can enhance the tumor-specific accumulation of NPs. Jing *et al.* modified HMPB NPs with HA-*g*-PEG copolymer in chemotherapy of breast cancer.[34] The HA-*g*-PEG surface coating of HMPB NPs prolonged their circulation time and enhanced their tumor targeting ability mediated by the CD44 receptor. Zhou *et al.* prepared HA-coated PB NPs for synergistic tumor therapy.[35] The HA-coated PB NPs exhibited specific uptake by tumor cells *in vitro* and targeting ability to tumor sites *in vivo*.

Red blood cell (RBC) and tumor cell membranes were also applied as surface camouflage for PB NPs. Chen *et al.* prepared RBC membrane-modified HMPB (HMPB@RBC) NPs for synergistic photothermal/chemotherapy of cancer (Fig. 4A).[36] After coating with the RBC membrane, the physiological stability, immune evading capacity, and blood retention time of HMPB@RBC NPs were significantly enhanced. *In vivo* pharmacokinetic curves showed that more HMPB@RBC NPs were retained in blood circulation at 24 h after intravenous injection (Fig. 4B). RBC membrane modification protected HMPB NPs from being cleared by the immune system. Moreover, extended blood retention time resulted in more accumulation in tumor through the enhanced permeability and retention (EPR) effect. Therefore, HMPB@RBC NPs exhibited lower distribution in spleen and higher distribution in tumors than HMPB NPs (Fig. 4C). Similarly, PB/MnO_2 NPs were also modified with the RBC membrane to enhance their *in vivo* circulation and drug loading capacity.[37] Liu *et al.* prepared HA@RBC@PB@CS-6 (HRPC) NPs to achieve targeted accumulation of CS-6 at tumor sites.[38] The modification of PB NPs with the RBC membrane extended the blood circulation time to 10 h and promoted the immune evasion ability by 60%. Moreover, HA was employed to achieve high concentration accumulation of HRPC NPs at tumor sites.

The tumor cell membrane will provide PB NPs with immune evasion ability and tissue-targeting ability. Chen *et al.* camouflaged HMPB@GOx (GPB) NPs with a murine mammary carcinoma (4T1) cell membrane (denoted as mGPB) to achieve homotypic targeting of GPB NPs.[39] Tumor fluorescence imaging (Fig. 4D) and bio-distribution (Fig. 4E) after the injection of DiR-labeled GPB and mGPB NPs indicated that the 4T1 membrane coating enhanced the immune evasion ability and homotypic targeting ability of GPB NPs.

Liposomes were also employed to modify PB NPs. Koshiyama *et al.* designed a liposome with a natural ion channel (composed

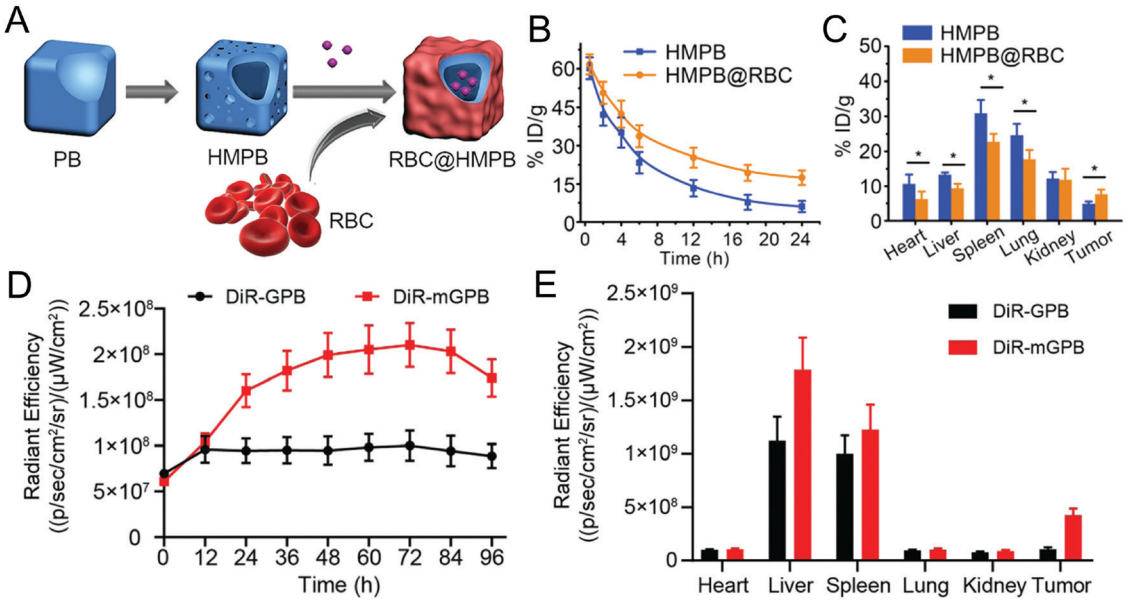

Fig. 4 PB NPs coated with the RBC membrane and 4T1 cell membrane. (A) Preparation of HMPB@RBC NPs. (B) *In vivo* pharmacokinetic curves after the intravenous injection of HMPB@RBC NPs. (C) Biodistribution of HMPB@RBC NPs at 24 h after injection. (A–C: adapted with permission from ref. 36. Copyright 2017, Wiley-VCH.) (D) Fluorescence of tumor tissue after the injection of mGPB and GPB. (E) Fluorescence of tumors and major organs at 96 h after injection. (D and E: adapted with permission from ref. 39. Copyright 2019, Royal Society of Chemistry).

of antibiotic amphotericin B) to adjust the influx rate of Fe^{2+} ions into the liposome encapsulating $Fe(CN)_6^{3-}$ ions.[40] The as-prepared PB NPs exhibited elevated adsorption performance toward Cs^+ ions. Uddin *et al.* reported that PB NPs embedded into a giant liposome membrane could serve as an ion transportation channel for OH^- influx.[41] Nevertheless, their biomedical applications were not explored.

2.5 PB-based nanocomposites

Integration with other nanomaterials is an efficient method to enhance and diversify the physicochemical properties of PB NPs. Currently, several PB-based nanocomposites with different physicochemical properties have been designed (Table 1), mainly focusing on drug delivery, photothermal properties, photodynamic properties, photoluminescence properties and X-ray absorption coefficient.

Original PB NPs are microporous, and exhibit limited loading capacity for drugs. Coating with mesoporous organosilica is a good option to increase the surface area of PB NPs. Tian *et al.* coated periodic mesoporous organosilica on PB NPs (denoted as PB@PMO).[42] The PB@PMO core–shell NPs possess a high surface area (866 $m^2\ g^{-1}$), mesoporous channels (3.2 nm) and high drug loading capacity (260 $\mu g\ mg^{-1}$).

Therapeutic efficiency is a main consideration in nanomaterials design. To elevate the photothermal conversion efficiency, Yu *et al.* designed $NaNdF_4$@PB core–shell NPs. The cross-relaxation pathway between Nd^{3+} ions and PB endowed the nanocomplexes with higher photothermal conversion efficiency compared to single $NaNdF_4$ and PB NPs.[43]

In addition to the photothermal effect, the photodynamic properties are also efficient to remove tumor cells and bacteria. A functional metal–organic framework (MOF) doped with porphyrin ligands could generate singlet oxygen in a photodynamic manner under 660 nm light illumination. Luo *et al.* coated the functional MOF shell on PB nanocubes, and the core–shell PB@MOF NPs showed remarkable synergistic photodynamic/photothermal properties under 660 nm and 808 nm dual light illumination to eradicate bacteria.[44]

Table 1 PB-based nanocomposites and their biomedical applications

Application	PB-based nanocomposites	Size (nm)	Year	Ref.
Drug delivery	PB@PMO core–shell NPs	125	2017	42
Photothermal therapy	$NaNdF_4$@PB core–shell NPs	29	2019	43
Chemodynamic therapy	Au@PB yolk–shell nanocubes	200	2019	51
Radiotherapy	Bi_2S_3 nanodots loaded in HMPB NPs	214	2020	48
Bacterial infection	PB@MOF core–shell nanocubes	300	2019	44
Optical imaging	$CuInS_2$–ZnS quantum dots attached to PB NPs	148	2017	45
	Carbon dots attached to PB NPs	100	2018	46
	$NaErF_4$@$NaYF_4$@$NaNdF_4$@PB multi-layer core–shell NPs	164	2019	47
Computed tomography	Bismuth PB NPs attached to BiOCl nanosheets	220	2019	49
	Au@PB core–shell NPs	18	2014	50

Optical imaging represents advanced imaging technologies for disease diagnosis and treatment. PB NPs lack suitable luminescence properties, which limits their application in optical imaging. It is a promising solution to construct nanocomposites combining luminescent components with therapeutic PB NPs. For instance, biocompatible $CuInS_2$–ZnS quantum dots (QDs) with NIR fluorescence emission[45] and carbon dots (CDs) with green photoluminescence emission[46] were attached to PB NPs to achieve optical imaging. Wang *et al.* designed a $NaErF_4$@$NaYF_4$@$NaNdF_4$@PB multi-layer core–shell nanocomposite; the $NaErF_4$ inner core provided this nanocomposite with intrinsic photoluminescence properties in the second window of NIR light.[47]

The X-ray adsorption of PB NPs is insufficient, which limits the application of PB NPs in radiotherapy and computed tomography (CT) imaging. Bismuth has a high X-ray attenuation coefficient, which matches well with radiotherapy and CT. Ren *et al.* encapsulated Bi_2S_3 nanodots (sensitizer) into HMPB NPs for radiotherapy.[48] Chen *et al.* attached NPs of the bismuth PB analog with BiOCl nanosheets to elevate the X-ray attenuation coefficient for CT imaging.[49] Similarly, Jing *et al.* prepared Au@PB core–shell nanocomposites with an elevated X-ray attenuation coefficient for CT imaging.[50] Hang *et al.* prepared Au@PB yolk-shell nanocubes for CT imaging and chemodynamic therapy.[51]

These novel structural designs have enabled PB-based NPs with more favorable physicochemical properties and extended their biomedical application.

3 Applications of PB-based NPs against various diseases

3.1 Treatment of inflammatory diseases

Inflammation is a natural response of the immune system to injury or infection. Clinical evidence indicates that excessive inflammation is adverse and is associated with many pathological dysfunctions.[52] The aberrant ROS generation is a significant mediator in the pathogenesis of inflammation.[53] Scavenging the overproduced ROS and regulating the following aberrant inflammatory response is a feasible approach to inhibit inflammation.[54–56]

Hydrogen peroxide, superoxide anions and hydroxyl radicals (•OH) are the main ROS in inflammatory diseases. In natural physiological conditions, antioxidative enzymes including POD, catalase (CAT) and superoxide dismutase (SOD) play a key role in scavenging hydrogen peroxide and superoxide anions and maintaining oxidative balance. The mixed-valence state provides PB-based NPs with multienzyme-like activities. Zhang *et al.* reported that PB NPs can mimic the activities of POD, SOD and CAT (Fig. 5).[57] As an anti-oxidative nanozyme, PB NPs can scavenge ROS and attenuate oxidative stress induced by stimuli like lipopolysaccharides and phorbol 12-myristate 13-acetate. Meanwhile, PB NPs can regulate the expression of inflammatory cytokines mediated by ROS. Generally, PB NPs are promising anti-inflammatory agents.

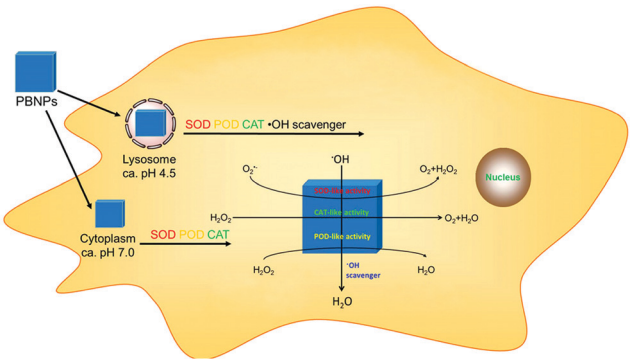

Fig. 5 The mechanism of PB NPs to scavenge ROS and regulate inflammation (adapted with permission from ref. 57. Copyright 2016, American Chemical Society).

Colitis and inflammatory bowel disease (IBD) are common inflammatory diseases. Zhao *et al.* used PVP-modified PB NPs to treat colitis.[58] PB NPs scavenged the overproduced ROS and downregulated the proinflammatory cytokines in a colitis mouse model induced by dextran sulfate sodium (DSS). Zhao *et al.* also synthesized manganese PB nanozymes (MPBZs) to treat IBD.[59] The MPBZs attenuated oxidative stress and inhibited inflammation. The pathological results of IBD mice after oral administration indicated the good anti-inflammatory effects of MPBZs.

PB NPs have also demonstrated their capabilities to attenuate neuroinflammation in nervous system injury and neurodegenerative diseases. Zhang *et al.* applied HPBZs in the treatment of ischemic stroke.[29] HPBZs exhibited excellent ROS-eliminating ability due to their multienzyme-like activities. Meanwhile, HPBZs could regulate inflammatory cytokine expression and suppress cell apoptosis effectively. SH-SY5Y (human neuroblastoma) cell assay and pathological results from a rat model indicated that HPBZ treatment could effectively scavenge ROS and counteract neuroinflammation in ischemic stroke. Alzheimer's disease is a complex neurodegenerative disease related to neuroinflammation and Tau-related pathology. Cai *et al.* prepared HMPWCs to attenuate Alzheimer's disease.[28] HMPWCs could scavenge ROS and suppress the activation of astrocytes and microglia to inhibit neuroinflammation. Meanwhile, the Tau-related pathology was inhibited by HMPWCs *via* the AKT/GSK-3β pathway. The synergistic effect contributed to the treatment of Alzheimer's disease.

These excellent works have clarified the anti-inflammatory therapeutic efficiency of PB-based NPs. Other PB-based nanomaterials also demonstrated their capacity to scavenge ROS and cure inflammatory disease. For instance, CuFe-PB NPs exhibited POD-like activity in the oxidation of dopamine, tyrosine and phenylalanine.[60,61] Copper PB analog NPs and VOx-doped Berlin Green (an oxidized state of PB) hydrogel exhibited enzyme-like activities to scavenge ROS.[62,63]

3.2 Application in tumor therapy

3.2.1 PTT. PB NPs has an absorbance peak of about 700 nm and a wide absorbance spectrum in the vis-NIR region.

Therefore, PB NPs can effectively convert NIR light into heat, leading to local hyperthermia and tumor cell death.[64] For instance, Hoffman *et al.* prepared PB NPs with a photothermal conversion efficiency of 20.5% for 808 nm light.[65] The remarkable photothermal effect of PB NPs underlies their application in PTT.[66]

The photothermal conversion efficiency of PB NPs is a significant consideration in PTT.[67] HMPB NPs exhibit extremely high photothermal conversion efficiency (41.4%) and a large molar extinction coefficient (1.2×10^{11} M^{-1} cm^{-1}) to an 808 nm laser.[110] To enhance the photothermal conversion efficiency, Yu *et al.* designed $NaNdF_4$@PB core–shell NPs.[43] The $NaNdF_4$@PB nanocomposites exhibited a higher tumor inhibition rate (76.7%) under an 808 nm laser than single $NaNdF_4$ (14.0%) and PB (18.8%) NPs.

Drugs were loaded into PB NPs to elevate the PTT efficiency. Heat shock proteins (HSPs) can repair heat-denatured proteins and are expressed in response to hyperthermia, which is a main obstacle hindering PTT. CS-6 can suppress the expression of HSP70 protein and reduce the thermal resistance of tumors. Liu *et al.* constructed HA@RBC@PB@CS-6 (HRPC) NPs to achieve enhanced PTT efficiency of breast cancer.[38] Plasmid DNA with HSP70 promoter was encapsulated into PB NPs to enhance the PTT of tumors.[68] A typical autophagy inhibitor, chloroquine, was also loaded into PB NPs to improve PTT efficiency.[69]

3.2.2 PDT. Hypoxia is a common feature in most solid tumors, which limits PDT efficacy and promotes tumor aggression.[70] Hence, attenuating hypoxia is a significant concern in tumor therapy.[71] As a catalase mimic, PB NPs can catalyze H_2O_2 decomposition and promote oxygen supply, which is beneficial for PDT.[72] Yang *et al.* encapsulated chlorin e6 (Ce6, photosensitizer) into PB@PMO NPs to achieve PDT.[73] PB catalyzed hydrogen peroxide decomposition into oxygen, and subsequently Ce6 transformed oxygen into singlet oxygen under 660 nm light irradiation to inhibit tumor growth. In this oxygen-evolving approach, the biocompatible PB@PMO@Ce6 nanoplatform showed remarkable PDT efficiency in tumor-bearing mice. Wang *et al.* designed mesoporous silica-coated PB (PSP) NPs for endogenous oxygen generation and imaging-guided PDT.[74] The PSP NPs were further loaded with zinc phthalocyanine (ZnPc, photosensitizer). Firstly, the inner PB NPs catalyzed endogenous H_2O_2 decomposition. Afterwards, ZnPc transformed oxygen into singlet oxygen under 671 nm light. Moreover, the PB core absorbed the 671 nm light and generated a synergistic photothermal effect.

DNA damage repair mechanisms including mutt homologue 1 (MTH1, a nucleotide pool sanitizing enzyme) of tumor cells are the main deficiencies of PDT. TH287 can inhibit the activity of MTH1 and elevate the DNA oxidative damage. Hu *et al.* prepared mesoporous organosilica-coated PB (PB@MSN) NPs to encapsulate tetraphenylporphyrin zinc (Zn-Por, photosensitizer) and TH287.[75] PB promoted oxygen supply and Zn-Por transformed oxygen into singlet oxygen under 660 nm laser irradiation to amplify oxidative damage to tumor cells. Meanwhile, TH287 suppressed MTH1-mediated damage repair and enhanced the oxidative damage in PDT (Fig. 6).

3.2.3 Chemotherapy. PB-based drug delivery systems, including HMPB NPs and mesoporous organosilica-coated PB NPs, exhibit a large surface area and remarkable loading capacity for antitumor drugs. Several PB-based systems have been designed for chemotherapy or synergistic tumor therapy.[76–79]

Typical antitumor drugs, such as doxorubicin (DOX), 10-hydroxycamptothecin and cisplatin, have been loaded into PB NPs for treatment of tumors.[34] For instance, Wu *et al.* loaded DOX into PB NPs for treatment of hepatocellular carcinoma.[80] Nevertheless, the tissue penetration depth is shallow, which limits the efficiency of antitumor drug. Losartan can degrade extracellular matrices and promote penetration of PB NPs. Zhang *et al.* encapsulated losartan and DOX into HMPB NPs to promote tumor tissue penetration.[81] The losartan co-encapsulation strategy allowed deep tissue penetration and high efficiency of DOX.

Response to the tumor microenvironment (TME) provides more diversity for tumor therapy.[82,83] The responsive behavior of PB-based NPs to stimuli including pH, temperature, NIR light and enzymes has been investigated.[84] The pH-responsive and temperature-responsive characteristics have good controllability, which is beneficial for smart drug release in tumor therapy.

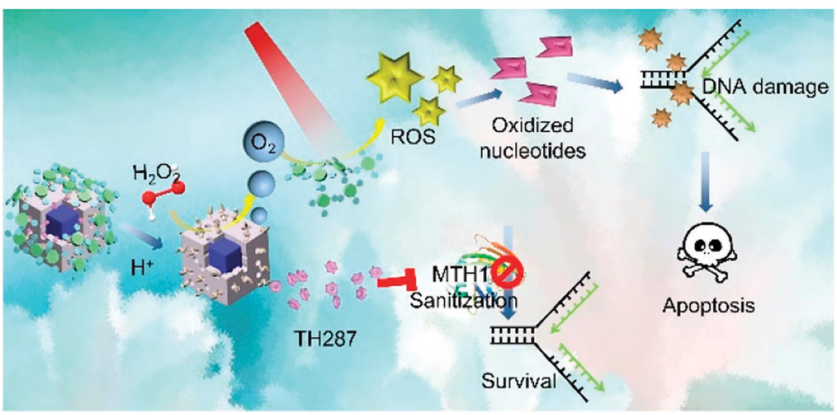

Fig. 6 The PDT and MTH1 inhibition on the PB@MSN nanoplatform (reprinted with permission from ref. 75. Copyright 2019, American Chemical Society).

PB-based NPs including HMPB, HMPB@RBC, manganese PB and NiCo-PB exhibit pH-responsive and photothermal-responsive release characters.[85,86] The mild acidity in the tumor environment and an exogenous NIR laser were applied as trigger to control drug release from PB-based NPs.

The pH-responsive ion release from PB analog NPs and doped PB NPs is also beneficial for tumor therapy. Since the bond between heteroatoms (such as Mn^{2+} and Cu^{2+}) and PB crystal is weak, the heteroatoms will be released gradually under low pH conditions. And the acid condition in the tumor microenvironment will be a proper trigger for metal ion release. Cai *et al.* constructed a manganese PB analog shell on HMPB NPs (denoted as HMPB@Mn).[20] The acid condition of the tumor microenvironment simultaneously triggered Mn^{2+} and DOX release from the core–shell nanocomposites. Hence, the pH-responsive released Mn^{2+} from HMPB@Mn was used as a MRI contrast agent to monitor synchronous DOX release.

The pH-responsive ion release of PB analog NPs was also used to generate antitumor drugs *via in situ* synthesis. Disulfiram (DSF) is a clinically approved alcohol-abuse drug and can be turned into an efficient antitumor drug, bis(*N*,*N*-diethyl dithiocarbamato)copper(II) (denoted as CuL_2). The CuL_2 complex possesses remarkable antitumor activity, but its high toxicity to normal tissues prevents its application in chemotherapy. Wu *et al.* designed copper-enriched HMPB NPs (Cu-HMPB) and provided an approach for *in situ* DSF-to-CuL_2 transformation (Fig. 7).[87] During DSF@PVP/Cu-HMPB accumulation in tumor tissue, the endogenous mild acidity in the tumor microenvironment triggers the synchronous release of DSF and Cu^{2+} from Cu-HMPB NPs, thus generating CuL_2 with antitumor activity.

3.2.4 Gas therapy. Gas therapy, especially remote-controllable gas therapy, is an emerging therapy for tumor treatment. To expand the biomedical application of carbon monoxide (CO), Li *et al.* designed a NIR-responsive CO-delivery system composed of mesoporous PB NPs, $Fe(CO)_5$ and PEG for treatment of tumors (Fig. 8).[88] Under 808 nm light irradiation, the photothermally induced high temperature prompts CO release from $Fe(CO)_5$. Moreover, $Fe(CO)_5$ is stable without NIR irradiation; therefore the NIR-responsive CO-release system will not cause acute CO poisoning.

The NIR-responsive CO-release system was used to reverse multidrug resistance and activate reductive drug. Multidrug resistance, associated with adenosine triphosphate (ATP)-dependent drug efflux, is a main factor limiting therapeutic efficiency in chemotherapy.[89] Li *et al.* employed this PB-based NIR-responsive CO-release system to reverse tumor resistance to DOX.[90] The released CO expedited mitochondrial metabolic exhaustion and inhibited ATP-dependent drug efflux. The results from a DOX-resistant MCF-7/ADR tumor model indicated that chemotherapy resistance to DOX is reversed. Meanwhile, Li *et al.* also applied this CO-release system to form a hypoxic condition for activation of reductive tirapazamine.[91] This PB-based NIR-responsive system was also employed to control nitric oxide (NO) release. Sodium nitroprusside ($Na_2Fe(CN)_5(NO)$, NO source) encapsulated into PB NPs released NO in tumor tissue under NIR light irradiation.[92]

3.2.5 Catalytic therapy. As a nanozyme, the enzyme-like activities of PB NPs can be used to construct cascade reactions for tumor therapy.[93] As a catalase mimic, HMPB NPs were combined with glucose oxidase (GOx) to form cascade reactions for starvation therapy.[94] The PB-mediated oxygen generation and GOx-mediated glucose depletion contributed to tumor starvation therapy. Moreover, glucose depletion could suppress the expression of HSPs and subsequently reduce tolerance to PTT.

Other therapies based on PB nanocomposites have also been reported. Ren *et al.* encapsulated bismuth sulfide nanodots (sensitizer) into HMPB NPs for radiotherapy.[48] Hang *et al.* prepared an Au@PB nanocomposite loaded with DOX for tumor diagnosis and chemodynamic therapy.[51] Odda *et al.* prepared PB-MoO_{3-x} NPs with synergistic PTT/PDT efficiency under 808 nm NIR light.[95] These multifunctional composites paved the way for diversified development of PB-based NPs.

3.3 Against bacterial infection

Bacterial infection presents a threat to healthcare worldwide. The long-term antibiotic abuse has resulted in the emergence and evolution of drug-resistant bacteria, which threaten the public health. For instance, in the treatment of *Staphylococcus aureus* (*S. aureus*)-related infection, the methicillin-resistant *S. aureus* (MRSA) strains have become a much more tough challenge to the current healthcare system. Therefore, it is necessary to develop excellent antibacterial therapy. PTT, converting the NIR light into heat to kill bacteria, is a promising candidate for bacterial infection and wound healing. PVP-coated PB NPs exhibited good photothermal ablation of *Escherichia coli* (*E. coli*) and MRSA under 980 nm laser irradiation.[96]

The photothermal conversion efficiency is a main factor limiting the photothermal therapeutic effects. The maximum absorbance peak of PB NPs is about 700 nm, and the deviation from ordinary 808 nm NIR light limits the conversion efficiency. Li *et al.* prepared three PB NPs with increasing zinc doping amounts (ZnPB-1, ZnPB-2 and ZnPB-3) to optimize the conversion efficiency (Fig. 9A).[97] After zinc doping, the absorbance peak

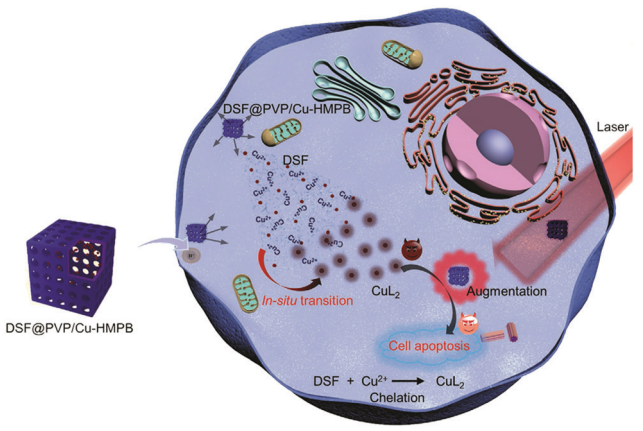

Fig. 7 Copper-enriched HMPB NPs for *in situ* CuL_2 transformation (adapted with permission from ref. 87. Copyright 2020, Wiley-VCH).

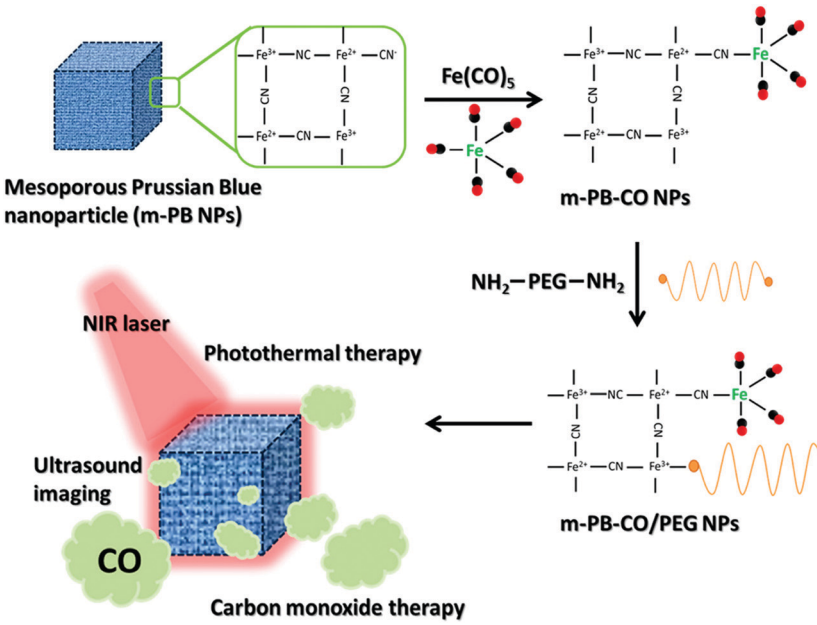

Fig. 8 PB-based NIR-responsive CO-release system (reprinted with permission from ref. 88. Copyright 2016, American Chemical Society).

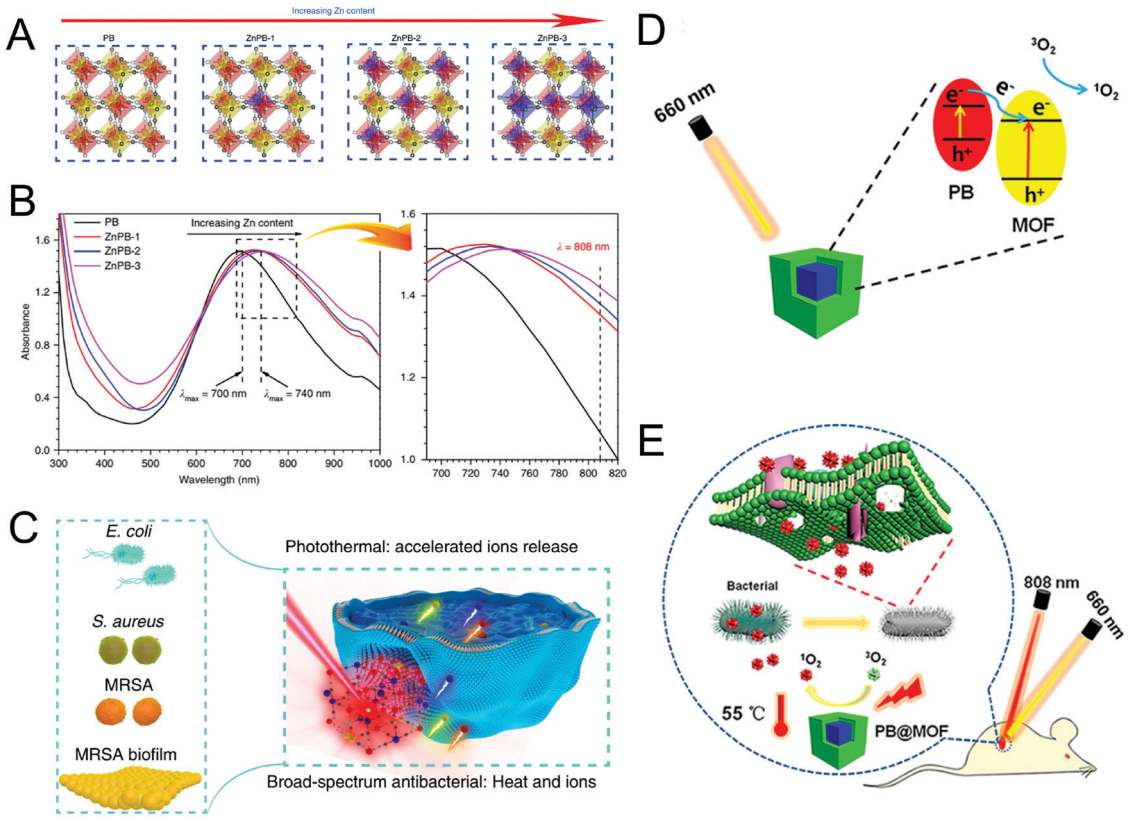

Fig. 9 Zinc-doped PB NPs and PB@MOF for bacterial infection and wound healing. (A) Structure of PB, ZnPB-1, ZnPB-2 and ZnPB-3. (B) UV-Vis-NIR spectrum of PB, ZnPB-1, ZnPB-2 and ZnPB-3. (C) Synergistic antibacterial mechanism of heat and ion release. (A–C: adapted with permission from ref. 97. Copyright 2019, Springer Nature.) (D) Photocatalytic mechanism of PB@MOF photocatalysts. (E) The bacterial killing of PB@MOF under dual light irradiation. (D and E: adapted with permission from ref. 44. Copyright 2019, American Chemical Society.)

shifted to 740 nm and the absorbance to 808 nm light was significantly improved, indicating the enhanced photothermal conversion efficiency (Fig. 9B). Theoretical calculation suggested that the enhanced photothermal conversion efficiency should be

ascribed to the bandgap-narrowing effect and the redshifted LSPR after zinc doping. ZnPB-3 NPs showed excellent antibacterial activity against *E. coli*, *S. aureus*, and MRSA biofilm. Meanwhile, the Fe^{3+}, Fe^{2+} and Zn^{2+} ion release accelerated by the local high temperature promoted collagen deposition and wound healing (Fig. 9C).

The antibacterial performance of PB-based nanocomposites was also investigated. Luo *et al.* synthesized a PB@MOF core–shell nanocomposite for bacterial infection and wound healing.[44] Porphyrin ligands in the metal–organic framework (MOF) shell prompted photocatalytic singlet oxygen generation under 660 nm light (Fig. 9D). Moreover, PB@MOF exhibited an enhanced photothermal conversion efficiency of 29.9% under an 808 nm laser. Under the illumination of 808 nm and 660 nm light, the PB@MOF nanocomposite exhibited an excellent antibacterial efficacy of 99.31% and 98.68% against *S. aureus* and *E. coli*, respectively (Fig. 9E).

Incorporating an antitumor component is also a way to enhance anti-bacterial therapy. Acetylcysteine (AC) could prevent the formation of a biofilm and inhibit bacterial adhesion on tissues. AC-decorated PB NPs eliminated 74% of *S. aureus* and 75% of *E. coli* under 980 nm NIR light.[98] Silver with outstanding antibacterial activity was also combined with PB NPs. Tong *et al.* applied PB@PDA@Ag composites to eradicate MRSA and accelerate diabetic wound healing.[99] Mukherjee *et al.* synthetized AgPB analog NPs and NiPB@Ag nanocomposites with antibacterial activities against *E. coli* and *Bacillus subtilis*.[100,101]

3.4 Bioimaging

Imaging plays a significant role in disease diagnosis and the following treatment. PB-based NPs perform well in MRI, PAI, ultrasound (US) imaging, and optical imaging after incorporating functional moieties including gadolinium, manganese and luminescent materials. PB-based NPs have been used to monitor the therapeutic effects and guide the treatment process.

MRI is a noninvasive medical imaging technique with high spatial resolution and deep tissue penetration.[102] PAI is a noninvasive imaging technique with excellent sensitivity, high resolution and real-time imaging capability.[103,104] PB NPs can act as a contrast agent in MRI and PAI,[105] but the efficiency of PB is lower than that of a clinical contrast agent. Incorporating Gd^{3+} and Mn^{2+} ions into PB is a good solution for optimization.[106] Considering this, hollow mesoporous gadolinium PB[22] and Mn^{2+}-doped PB NPs[107] were prepared to achieve enhanced bimodal MRI/PAI performance. Furthermore, the MRI/PAI imaging of PB@PMO NPs was used to guide synergistic photothermal/chemotherapy of triple negative breast cancer (Fig. 10A and B).[42] And the MRI of zinc-doped ultrasmall PB NPs was used to guide the PTT of breast cancer.[30]

It is noteworthy that poly-L-lysine-coated PB NPs were applied as a cell label to achieve the PAI of human mesenchymal stem cells.[108] Stem cell therapy is efficient in the treatment of traumatic brain injury (TBI). Li *et al.* used PB NPs to label bone mesenchymal stem cells (BMSCs) to monitor TBI rehabilitation.[109] Meanwhile, BMSCs are capable of overcoming

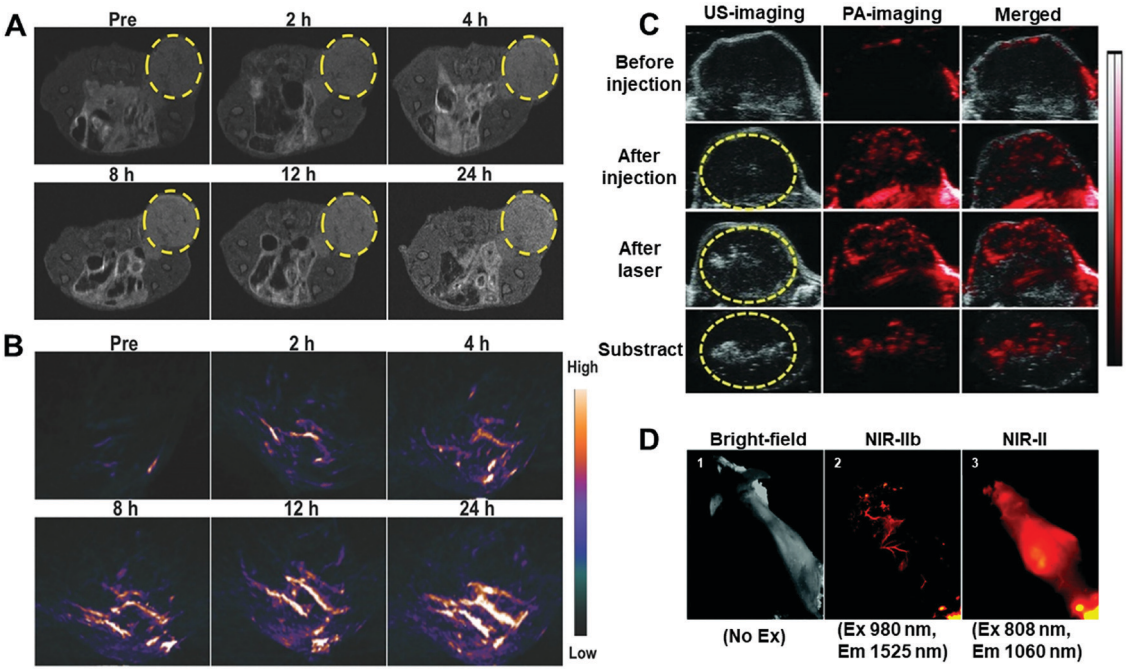

Fig. 10 Bioimaging performance of PB-based NPs. (A) MRI images and (B) PAI images of tumor-bearing mice at different times after the injection of PB@PMO-Cy5.5 NPs. (A and B: reprinted with permission from ref. 42. Copyright 2016, the authors.) (C) US images and PAI images of tumor tissue before and after the injection of HMPB-PFP NPs (adapted with permission from ref. 111. Copyright 2015, Wiley-VCH). (D) NIR-II fluorescence imaging of a mouse after the injection of $NaErF_4$@$NaYF_4$@$NaNdF_4$@PB NPs under 980 nm or 808 nm laser irradiation (adapted with permission from ref. 47. Copyright 2019, Royal Society of Chemistry)

the blood–brain barrier and enhance PB NP penetration into the brain parenchyma.

US imaging is a noninvasive low-cost imaging technique with real-time imaging capability. Perfluoropentane (PFP), which will undergo liquid–gas transformation at high temperature, is an excellent contrast agent for US imaging. Hollow cavities are suitable for PFP encapsulation, and the high temperature in PTT is a proper trigger for PFP transformation. Cai *et al.* encapsulated PFP and DOX into HMPB NPs to monitor the efficiency of synergistic PTT/chemotherapy with US imaging and PAI (Fig. 10C).[110,111]

PB NPs are not luminescent, so it is necessary to incorporate biocompatible luminescent materials to achieve optical imaging. For instance, the $NaErF_4$@$NaYF_4$@$NaNdF_4$@PB nanocomposites were designed for high-resolution NIR (1525 nm) optical imaging of the blood vessels and tumors under 980 nm laser excitation (Fig. 10D).[47]

Other imaging modes about PB have also been investigated. Promdet *et al.* prepared manganese PB analogs for CT.[112] Liu *et al.* employed lutetium-doped $NaDyF_4$ NPs as the core of PB nanocomposites to achieve multifunctional CT/MRI-guided PTT.[113] PB NPs labeled with ^{201}Tl were applied in single photon emission computed tomography.[114,115] Zhu *et al.* prepared PB NPs for zero-background surface-enhanced Raman scattering imaging with remarkable spatial resolution and depth.[116] Apart from therapeutic guidance, the magnetic targeting ability of PB-based NPs (for example, Fe_3O_4@PB) was also reported.[117] The above-mentioned structures enabled PB-based NPs with more promising features in biomedicine.

4. Conclusions and future perspective

In summary, this review article provides a comprehensive report of PB-based NPs and their biomedical applications. In the past decade, the basic physicochemical characteristics of PB-based NPs, including photothermal effect, enzyme-like activity and drug delivery capability, have been systematically investigated. Several novel design strategies for PB-based NPs were applied to achieve extended blood circulation, tumor tissue-targeting, TME-responsive ion release and *in situ* drug synthesis. Owing to these novel design strategies, PDT and synergistic therapy exhibited excellent therapeutic efficiency in the treatment of tumors and bacterial infection. Meanwhile, NPs of PB-based nanozymes have demonstrated their therapeutic efficiency for inflammatory disease due to their remarkable ROS-scavenging capability.

Previous studies of PB-based NPs will navigate the future development. Diversified design is a developing orientation of PB-based NPs. Currently, zinc/gadolinium-doped PB NPs with enhanced photothermal efficiency, PB@MOF nanocomposites with synergistic PDT/PTT efficiency and PB-based NIR-responsive gas therapy have been designed for tumor therapy or bacterial infection treatment. However, the light sources applied in the above-mentioned PTT and NIR-responsive system are in the first NIR window (NIR-I), and lack adequate tissue penetration depth and spatial resolution. To overcome this deficiency of PB NPs, it is necessary to further tune their adsorption spectrum toward the second NIR window (NIR-II) and incorporate materials with intrinsic adsorption to NIR-II light (for instance, conjugated polymers).

Besides, there is inadequate research on blood circulation, tissue penetration, cell uptake, and intracellular metabolism of PB-based NPs, which leads to controversy in therapeutic mechanisms and debates regarding their clinical translation. For instance, the structural integrity of PB-based NPs shall be adjustable according to different therapeutic modalities and different steps in one modality. Therefore, a careful study on the interactions of PB-based NPs with different tissues, cells and cellular organelles shall be carried out.

Conflicts of interest

The authors declare that no competing interest exists.

Acknowledgements

We acknowledge the financial support of the National Natural Science Foundation of China (51822306, 51973187), the National Key Research and Development Program of China (2016YFE0132700), and the Fundamental Research Funds for the Central Universities of China.

References

1 Z. Y. Yu, Y. Duan, J. D. Liu, Y. Chen, X. K. Liu, W. Liu, T. Ma, Y. Li, X. S. Zheng, T. Yao, M. R. Gao, J. F. Zhu, B. J. Ye and S. H. Yu, *Nat. Commun.*, 2019, **10**, 2799, DOI: 10.1038/s41467-019-10698-9.
2 W. Wang, Y. Gang, Z. Hu, Z. Yan, W. Li, Y. Li, Q. F. Gu, Z. Wang, S. L. Chou, H. K. Liu and S. X. Dou, *Nat. Commun.*, 2020, **11**, 980, DOI: 10.1038/s41467-020-14444-4.
3 M. Atzori, I. Breslavetz, K. Paillot, K. Inoue, G. L. J. A. Rikken and C. Train, *J. Am. Chem. Soc.*, 2019, **141**, 20022–20025.
4 B. Kong, C. Selomulya, G. Zheng and D. Zhao, *Chem. Soc. Rev.*, 2015, **44**, 7997–8018.
5 Z. Qin, Y. Li and N. Gu, *Adv. Healthcare Mater.*, 2018, **7**, 1800347.
6 J. F. Keggin and F. D. Miles, *Nature*, 1936, **137**, 577.
7 H. J. Buser, D. Schwarzenbach, W. Petter and A. Ludi, *Inorg. Chem.*, 1977, **16**, 2704–2710.
8 FDA News: FDA Approves First New Drug Application for Treatment of Radiation Contamination due to Cesium or Thallium, 2003, https://www.fda.gov/drugs/bioterrorism-and-drug-preparedness/fda-approves-first-new-drug-application-treatment-radiation-contamination-due-cesium-or-thallium.
9 G. Fu, W. Liu, S. Feng and X. Yue, *Chem. Commun.*, 2012, **48**, 11567–11569.
10 G. C. Yu, S. Yu, M. Saha, J. Zhou, T. R. Cook, B. C. Yung, J. Chen, Z. W. Mao, F. W. Zhang, Z. J. Zou, Y. J. Liu, L. Shao,

S. Wang, C. Y. Gao, F. H. Huang, P. J. Stang and X. Y. Chen, *Nat. Commun.*, 2018, **9**, 4335, DOI: 10.1038/s41467-018-06574-7.
11 T. Uemura and S. Kitagawa, *J. Am. Chem. Soc.*, 2003, **125**, 7814–7815.
12 H. Fujita, H. Sasano, R. Miyajima and A. Sakoda, *Adsorption*, 2014, **20**, 905–915.
13 X. Shen, S. Wu, Y. Liu, K. Wang, Z. Xu and W. Liu, *J. Colloid Interface Sci.*, 2009, **329**, 188–195.
14 Y. Ding, Y. Hu, G. Gu and X. Xia, *J. Phys. Chem. C*, 2009, **113**, 14838–14843.
15 F. Shiba, U. Mameuda, S. Tatejima and Y. Okawa, *RSC Adv.*, 2019, **9**, 34589–34594.
16 Z. Qin, B. Chen, X. Huang, Y. Mao, Y. Li, F. Yang and N. Gu, *Dalton Trans.*, 2019, **48**, 17169–17173.
17 M. A. Komkova, E. E. Karyakina and A. A. Karyakin, *J. Am. Chem. Soc.*, 2018, **140**, 11302–11307.
18 M. S. Kandanapitiye, B. Valley, L. D. Yang, A. M. Fry, P. M. Woodward and S. D. Huang, *Inorg. Chem.*, 2013, **52**, 2790–2792.
19 C. Zhao, B. Liu, X. Li, K. Zhu, R. Hu, Z. Ao and J. Wang, *Chem. Commun.*, 2019, **55**, 7151.
20 X. Cai, W. Gao, M. Ma, M. Wu, L. Zhang, Y. Zheng, H. Chen and J. Shi, *Adv. Mater.*, 2015, **27**, 6382–6389.
21 M. F. Dumont, H. A. Hoffman, P. R. S. Yoon, L. S. Conklin, S. R. Saha, J. Paglione, R. W. Sze and R. Fernandes, *Bioconjugate Chem.*, 2014, **25**, 129–137.
22 X. Cai, W. Gao, L. Zhang, M. Ma, T. Liu, W. Du, Y. Zheng, H. Chen and J. Shi, *ACS Nano*, 2016, **10**, 11115–11126.
23 G. Liang, J. Xu and X. Wang, *J. Am. Chem. Soc.*, 2009, **131**, 5378–5379.
24 X. Roy, J. K. Hui, M. Rabnawaz, G. Liu and M. J. Maclachlan, *J. Am. Chem. Soc.*, 2011, **133**, 8420–8423.
25 M. Hu, S. Furukawa, R. Ohtani, H. Sukegawa, Y. Nemoto, J. Reboul, S. Kitagawa and Y. Yamauchi, *Angew. Chem., Int. Ed.*, 2012, **51**, 984–988.
26 M. Hu, A. A. Belik, M. Imura and Y. Yamauchi, *J. Am. Chem. Soc.*, 2013, **135**, 384–391.
27 W. Zhang, Y. Zhao, V. Malgras, Q. Ji, D. Jiang, R. Qi, K. Ariga, Y. Yamauchi, J. Liu, J. Sen Jiang and M. Hu, *Angew. Chem., Int. Ed.*, 2016, **55**, 8228–8234.
28 X. Cai, K. Zhang, X. Xie, X. Zhu, J. Feng, Z. Jin, H. Zhang, M. Tian and H. Chen, *Biomaterials*, 2020, **231**, 119678.
29 K. Zhang, M. Tu, W. Gao, X. Cai, F. Song, Z. Chen, Q. Zhang, J. Wang, C. Jin, J. Shi, X. Yang, Y. Zhu, W. Gu, B. Hu, Y. Zheng, H. Zhang and M. Tian, *Nano Lett.*, 2019, **19**, 2812–2823.
30 P. Shou, Z. Yu, Y. Wu, Q. Feng, B. Zhou, J. Xing, C. Liu, J. Tu, O. U. Akakuru, Z. Ye, X. Zhang, Z. Lu, L. Zhang and A. Wu, *Adv. Healthcare Mater.*, 2020, **9**, 1900948.
31 M. Hu, N. L. K. Torad, Y. D. Chiang, K. C. W. Wu and Y. Yamauchi, *CrystEngComm*, 2012, **14**, 3387–3396.
32 L. Cheng, H. Gong, W. Zhu, J. Liu, X. Wang, G. Liu and Z. Liu, *Biomaterials*, 2014, **35**, 9844–9852.
33 P. Xue, L. Sun, Q. Li, L. Zhang, Z. Xu, C. Ming Li and Y. Kang, *J. Colloid Interface Sci.*, 2018, **509**, 384–394.
34 L. Jing, S. Shao, Y. Wang, Y. Yang, X. Yue and Z. Dai, *Theranostics*, 2016, **6**, 40–53.
35 B. Zhou, B. Jiang, W. Sun, F. Wei, Y. He, H. Liang and X. Shen, *ACS Appl. Mater. Interfaces*, 2018, **10**, 18036–18049.
36 W. Chen, K. Zeng, H. Liu, J. Ouyang, L. Wang, Y. Liu, H. Wang, L. Deng and Y. Liu, *Adv. Funct. Mater.*, 2017, **27**, 1605795.
37 J. Peng, Q. Yang, W. Li, L. Tan, Y. Xiao, L. Chen, Y. Hao and Z. Qian, *ACS Appl. Mater. Interfaces*, 2017, **9**, 44410–44422.
38 B. Liu, W. Wang, J. Fan, Y. Long, F. Xiao, M. Daniyal, C. Tong, Q. Xie, Y. Jian, B. Li, X. Ma and W. Wang, *Biomaterials*, 2019, **217**, 119301.
39 Y. Chen, Z. H. Li, J. J. Hu, S. Y. Peng, L. Rong, Y. Sun and X. Z. Zhang, *Nanoscale Horiz.*, 2020, **5**, 283–293.
40 T. Koshiyama, M. Tanaka, M. Honjo, Y. Fukunaga, T. Okamura and M. Ohba, *Langmuir*, 2018, **34**, 1666–1672.
41 S. M. N. Uddin, S. Laokroekkiat, M. A. Rashed, S. Mizuno, K. Ono, M. Ishizaki, K. Kanaizuka, M. Kurihara, Y. Nagao and T. Hamada, *Chem. Commun.*, 2020, **56**, 1046–1049.
42 W. Tian, Y. Su, Y. Tian, S. Wang, X. Su, Y. Liu, Y. Zhang, Y. Tang, Q. Ni, W. Liu, M. Dang, C. Wang, J. Zhang, Z. Teng and G. Lu, *Adv. Sci.*, 2017, **4**, 1600356.
43 Z. Yu, W. Hu, H. Zhao, X. Miao, Y. Guan, W. Cai, Z. Zeng, Q. Fan and T. T. Y. Tan, *Angew. Chem., Int. Ed.*, 2019, **58**, 8536.
44 Y. Luo, J. Li, X. Liu, L. Tan, Z. Cui, X. Feng, X. Yang, Y. Liang, Z. Li, S. Zhu, Y. Zheng, K. W. K. Yeung, C. Yang, X. Wang and S. Wu, *ACS Cent. Sci.*, 2019, **5**, 1591–1601, DOI: 10.1021/acscentsci.9b00639.
45 Y. Yang, L. Jing, X. Li, L. Lin, X. Yue and Z. Dai, *Theranostics*, 2017, **7**, 466–481.
46 X. Peng, R. Wang, T. Wang, W. Yang, H. Wang, W. Gu and L. Ye, *ACS Appl. Mater. Interfaces*, 2018, **10**, 1084–1092.
47 X. Wang, H. Li, F. Li, X. Han and G. Chen, *Nanoscale*, 2019, **11**, 22079–22088.
48 C. Ren, Y. Cheng, W. Li, P. Liu, L. Yang, Q. Lu, M. Xu, F. Tan, J. Li and N. Li, *Biomater. Sci.*, 2020, **8**, 1981–1995.
49 X. Chen, R. Wang, D. Liu, Y. Tian and L. Ye, *ACS Appl. Bio. Mater.*, 2019, **2**, 1213–1224.
50 L. Jing, X. Liang, Z. Deng, S. Feng, X. Li, M. Huang, C. Li and Z. Dai, *Biomaterials*, 2014, **35**, 5814–5821.
51 L. Hang, H. Li, T. Zhang, D. Men, C. Zhang, P. Gao and Q. Zhang, *ACS Appl. Mater. Interfaces*, 2019, **11**, 39493–39502.
52 I. F. Charo and R. M. Ransohoff, *N. Engl. J. Med.*, 2006, **354**, 610–621.
53 K. Zhang and R. J. Kaufman, *Nature*, 2008, **454**, 455–462.
54 B. Yang, Y. Chen and J. Shi, *Chem. Rev.*, 2019, **119**, 4881–4985.
55 Y. J. Yao, J. Ding, Z. Y. Wang, H. L. Zhang, J. Q. Xie, Y. C. Wang, L. J. Hong, Z. W. Mao, J. Q. Gao and C. Y. Gao, *Biomaterials*, 2020, **232**, 119726.
56 Y. W. Chen, W. L. Shen, C. Q. Tang, J. Y. Huang, C. M. Fan, Z. Yin, Y. J. Hu, W. S. Chen, H. W. Ouyang, Y. T. Zhou, Z. W. Mao and X. Chen, *Sci. Adv.*, 2020, **6**, eaay9526.
57 W. Zhang, S. Hu, J. J. Yin, W. He, W. Lu, M. Ma, N. Gu and Y. Zhang, *J. Am. Chem. Soc.*, 2016, **138**, 5860–5865.

58 J. Zhao, X. Cai, W. Gao, L. Zhang, D. Zou, Y. Zheng, Z. Li and H. Chen, *ACS Appl. Mater. Interfaces*, 2018, **10**, 26108–26117.
59 J. Zhao, W. Gao, X. Cai, J. Xu, D. Zou, Z. Li, B. Hu and Y. Zheng, *Theranostics*, 2019, **9**, 2843–2855.
60 M. Vázquez-González, R. M. Torrente-Rodríguez, A. Kozell, W. C. Liao, A. Cecconello, S. Campuzano, J. M. Pingarrón and I. Willner, *Nano Lett.*, 2017, **17**, 4958–4963.
61 J. Hou, M. Vázquez-González, M. Fadeev, X. Liu, R. Lavi and I. Willner, *Nano Lett.*, 2018, **18**, 4015–4022.
62 R. Zhou, P. Wang, Y. Guo, X. Dai, S. Xiao, Z. Fang, R. Speight, E. W. Thompson, P. J. Cullen and K. K. Ostrikov, *Nanoscale*, 2019, **11**, 19497–19505.
63 S. Sahar, A. Zeb, C. Ling, A. Raja, G. Wang, N. Ullah, X. Lin and A. Xu, *ACS Nano*, 2020, **14**, 3017–3031.
64 G. C. Yu, Z. Yang, X. Fu, B. C. Yung, J. Yang, Z. W. Mao, L. Shao, B. Hua, Y. J. Liu, F. W. Zhang, Q. L. Fan, S. Wang, O. Jacobson, A. Jin, C. Y. Gao, X. Y. Tang, F. H. Huang and X. Y. Chen, *Nat. Commun.*, 2018, **9**, 766, DOI: 10.1038/s41467-018-03119-w.
65 H. A. Hoffman, L. Chakrabarti, M. F. Dumont, A. D. Sandler and R. Fernandes, *RSC Adv.*, 2014, **4**, 29729–29734.
66 Z. Li, Y. Zeng, D. Zhang, M. Wu, L. Wu, A. Huang, H. Yang, X. Liu and J. Liu, *J. Mater. Chem. B*, 2014, **2**, 3686–3696.
67 C. X. Bi, J. Chen, Y. Chen, Y. Song, A. R. Li, S. Z. Li, Z. W. Mao, C. Y. Gao, D. Y. Wang, H. Moehwald and H. B. Xia, *Chem. Mater.*, 2018, **30**, 2709–2718.
68 Y. Liu, G. Shu, X. Li, H. Chen, B. Zhang, H. Pan, T. Li, X. Gong, H. Wang, X. Wu, Y. Dou and J. Chang, *Adv. Funct. Mater.*, 2018, **28**, 1802026.
69 Y. Ma, H. Chen, B. Hao, J. Zhou, G. He, Z. Miao, Y. Xu, L. Gao, W. Zhou and Z. Zha, *J. Mater. Chem. B*, 2018, **6**, 5854–5859.
70 G. C. Yu, B. Y. Zhu, L. Shao, J. Zhou, M. L. Saha, B. B. Shi, Z. B. Zhang, T. Hong, S. J. Li, X. Y. Chen and P. J. Stang, *Proc. Natl. Acad. Sci. U. S. A.*, 2019, **116**, 6618–6623.
71 H. T. Z. Zhu, H. H. Wang, B. B. Shi, L. Q. Shangguan, W. J. Tong, G. C. Yu, Z. W. Mao and F. H. Huang, *Nat. Commun.*, 2019, **10**, 2412, DOI: 10.1038/s41467-019-10385-9.
72 Z. M. He, X. L. Huang, C. Wang, X. L. Li, Y. J. Liu, Z. J. Zhou, S. Wang, F. W. Zhang, Z. T. Wang, O. Jacobson, J.-J. Zhu, G. C. Yu, Y. L. Dai and X. Y. Chen, *Angew. Chem., Int. Ed.*, 2019, **58**, 8752–8756.
73 Z. L. Yang, W. Tian, Q. Wang, Y. Zhao, Y. L. Zhang, Y. Tian, Y. X. Tang, S. J. Wang, Y. Liu, Q. Q. Ni, G. M. Lu, Z. G. Teng and L. J. Zhang, *Adv. Sci.*, 2018, **5**, 1700847.
74 D. Wang, R. Shi, J. Zhou, S. Shi, H. Wu, P. Xu, H. Wang, G. Xia, T. E. Barnhart, W. Cai, Z. Guo and Q. Chen, *iScience*, 2018, **9**, 14–26.
75 J. J. Hu, Y. Chen, Z. H. Li, S. Y. Peng, Y. Sun and X. Z. Zhang, *Nano Lett.*, 2019, **19**, 5568–5576.
76 H. Chen, Y. Ma, X. Wang and Z. Zha, *J. Mater. Chem. B*, 2017, **5**, 7051–7058.
77 H. Chen, Y. Ma, X. Wang, X. Wu and Z. Zha, *RSC Adv.*, 2017, **7**, 248–255.
78 Y. Su, Z. Teng, H. Yao, S. Wang, Y. Tian, Y. Zhang, W. Liu, W. Tian, L. Zheng, N. Lu, Q. Ni, X. Su, Y. Tang, J. Sun, Y. Liu, J. Wu, G. Yang, G. Lu and L. Zhang, *ACS Appl. Mater. Interfaces*, 2016, **8**, 17038–17046.
79 M. Gautam, B. K. Poudel, Z. C. Soe, K. Poudel, S. Maharjan, S. K. Ku, C. S. Yong, S. W. Joo, J. O. Kim and J. H. Byeon, *Chem. Eng. J.*, 2020, **383**, 123177.
80 M. Wu, Q. Wang, X. Liu and J. Liu, *RSC Adv.*, 2015, **5**, 30970–30980.
81 Y. Zhang, Y. Liu, X. Gao, X. Li, X. Niu, Z. Yuan and W. Wang, *Acta Biomater.*, 2019, **90**, 314–323.
82 G. C. Yu, X. L. Zhao, J. Zhou, Z. W. Mao, X. L. Huang, Z. T. Wang, B. Hua, Y. J. Liu, F. W. Zhang, Z. M. He, O. Jacobson, C. Y. Gao, W. L. Wang, C. Y. Yu, X. Y. Zhu, F. H. Huang and X. Y. Chen, *J. Am. Chem. Soc.*, 2018, **140**, 8005–8019.
83 S. Wang, G. C. Yu, Z. T. Wang, O. Jacobson, R. Tian, L.-S. Lin, F. W. Zhang, J. Wang and X. Y. Chen, *Adv. Mater.*, 2018, **30**, 1803926.
84 P. Xue, K. K. Y. Cheong, Y. Wu and Y. Kang, *Colloids Surf., B*, 2015, **125**, 277–283.
85 Q. Jia, F. Su, Z. Li, X. Huang, L. He, M. Wang, Z. Zhang, S. Fang and N. Zhou, *ACS Appl. Bio. Mater.*, 2019, **2**, 2143–2154.
86 Q. Jia, Z. Li, C. Guo, X. Huang, M. Kang, Y. Song, L. He, N. Zhou, M. Wang, Z. Zhang, G. Fu and M. Du, *Chem. Eng. J.*, 2020, **389**, 124468.
87 W. Wu, L. Yu, Y. Pu, H. Yao, Y. Chen and J. Shi, *Adv. Mater.*, 2020, 2000542.
88 W. P. Li, C. H. Su, L. C. Tsao, C. T. Chang, Y. P. Hsu and C. S. Yeh, *ACS Nano*, 2016, **10**, 11027–11036.
89 G. C. Yu, B. C. Yung, Z. Zhou, Z. W. Mao and X. Y. Chen, *ACS Nano*, 2018, **12**, 7–12.
90 Y. Li, J. Dang, Q. Liang and L. Yin, *ACS Cent. Sci.*, 2019, **5**, 1044–1058.
91 Y. Li, J. Dang, Q. Liang and L. Yin, *Biomaterials*, 2019, **209**, 138–151.
92 T. Feng, J. Wan, P. Li, H. Ran, H. Chen, Z. Wang and L. Zhang, *Biomaterials*, 2019, **214**, 119213.
93 Z. G. Ren, S. C. Sun, R. R. Sun, G. Y. Cui, L. J. Hong, B. C. Rao, A. Li, Z. J. Yu, Q. C. Kan and Z. W. Mao, *Adv. Mater.*, 2019, 1906024.
94 J. Zhou, M. Li, Y. Hou, Z. Luo, Q. Chen, H. Cao, R. Huo, C. Xue, L. Sutrisno, L. Hao, Y. Cao, H. Ran, L. Lu, K. Li and K. Cai, *ACS Nano*, 2018, **12**, 2858–2872.
95 A. H. Odda, Y. Xu, J. Lin, G. Wang, N. Ullah, A. Zeb, K. Liang, L. P. Wen and A. W. Xu, *J. Mater. Chem. B*, 2019, **7**, 2032–2042.
96 H. Maaoui, R. Jijie, G. H. Pan, D. Drider, D. Caly, J. Bouckaert, N. Dumitrascu, R. Chtourou, S. Szunerits and R. Boukherroub, *J. Colloid Interface Sci.*, 2016, **480**, 63–68.
97 J. Li, X. Liu, L. Tan, Z. Cui, X. Yang, Y. Liang, Z. Li, S. Zhu, Y. Zheng, K. W. K. Yeung, X. Wang and S. Wu, *Nat. Commun.*, 2019, **10**, 4490.
98 S. Cai, J. Qian, S. Yang, L. Kuang and D. Hua, *Colloids Surf., B*, 2019, **181**, 31–38.
99 C. Tong, X. Zhong, Y. Yang, X. Liu, G. Zhong, C. Xiao, B. Liu, W. Wang and X. Yang, *Biomaterials*, 2020, **243**, 119936.

100 S. Mukherjee, R. Kotcherlakota, S. Haque, S. Das, S. Nuthi, D. Bhattacharya, K. Madhusudana, S. Chakravarty, R. Sistla and C. R. Patra, *ACS Biomater. Sci. Eng.*, 2020, **6**, 690–704.
101 S. Mukherjee, S. Das, S. Nuthi and C. R. Patra, *Future Sci. OA*, 2017, **3**(4), FSO233.
102 E. Terreno, D. D. Castelli, A. Viale and S. Aime, *Chem. Rev.*, 2010, **110**, 3019–3042.
103 C. Kim, C. Favazza and L. Wang, *Chem. Rev.*, 2010, **110**, 2756–2782.
104 G. C. Yu, J. Yang, X. Fu, Z. T. Wang, L. Shao, Z. W. Mao, Y. J. Liu, Z. Yang, F. W. Zhang, W. Fan, J. B. Song, Z. J. Zhou, C. Y. Gao, F. H. Huang and X. Y. Chen, *Mater. Horiz.*, 2018, **5**, 429–435.
105 X. Liang, Z. Deng, L. Jing, X. Li, Z. Dai, C. Li and M. Huang, *Chem. Commun.*, 2013, **49**, 11029–11031.
106 L. Fétiveau, G. Paul, A. Nicolas-boluda, J. Volatron, R. George, S. Laurent, R. Muller, L. Sancey, P. Mejanelle, A. Gloter and L. Catala, *Chem. Commun.*, 2019, **55**, 14844.
107 W. Zhu, K. Liu, X. Sun, X. Wang, Y. Li, L. Cheng and Z. Liu, *ACS Appl. Mater. Interfaces*, 2015, **7**, 11575–11582.
108 T. Kim, J. E. Lemaster, F. Chen, J. Li and J. V. Jokerst, *ACS Nano*, 2017, **11**, 9022–9032.
109 W. Li, R. Chen, J. Lv, H. Wang, Y. Liu, Y. Peng, Z. Qian, G. Fu and L. Nie, *Adv. Sci.*, 2017, 1700277.
110 X. Jia, X. Cai, Y. Chen, S. Wang, H. Xu, K. Zhang, H. Wu, J. Shi and H. Chen, *ACS Appl. Mater. Interfaces*, 2015, **7**, 4579–4588.
111 X. Cai, X. Jia, W. Gao, K. Zhang, M. Ma, S. Wang, Y. Zheng, J. Shi and H. Chen, *Adv. Funct. Mater.*, 2015, **25**, 2520–2529.
112 P. Promdet, B. Rodríguez-García, A. Henry, C. Nguyen, T. Khuu, J. R. Galan-Mascaros and K. Sorasaenee, *Dalton Trans.*, 2018, **47**, 11960–11967.
113 Y. Liu, Q. Guo, X. Zhu, W. Feng, L. Wang, L. Ma, G. Zhang, J. Zhou and F. Li, *Adv. Funct. Mater.*, 2016, **26**, 5120–5130.
114 M. Perrier, M. Busson, G. Massasso, J. Long, V. Boudousq, J. P. Pouget, S. Peyrottes, C. Perigaud, C. Porredon-Guarch, J. De Lapuente, M. Borras, J. Larionova and Y. Guari, *Nanoscale*, 2014, **6**, 13425–13429.
115 G. Maurin-Pasturel, E. Rascol, M. Busson, S. Sevestre, J. Lai-Kee-Him, P. Bron, J. Long, J. Chopineau, J. M. Devoisselle, Y. Guari and J. Larionova, *Inorg. Chem. Front.*, 2017, **4**, 1737–1741.
116 W. Zhu, M. Y. Gao, Q. Zhu, B. Chi, L. W. Zeng, J. M. Hu and A. G. Shen, *Nanoscale*, 2020, **12**, 3292–3301.
117 G. Fu, W. Liu, Y. Li, Y. Jin, L. Jiang, X. Liang, S. Feng and Z. Dai, *Bioconjugate Chem.*, 2014, **25**, 1655–1663.